

Visualization of Multifractal Superconductivity in a Two-Dimensional Transition Metal Dichalcogenide in the Weak-Disorder Regime

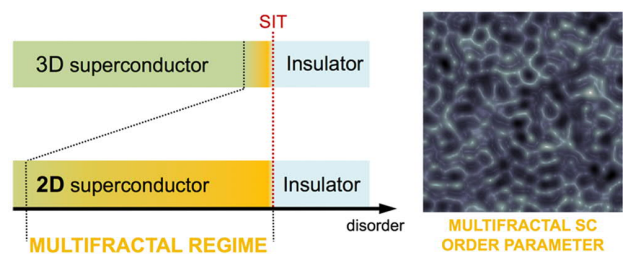
Carmen Rubio-Verdú, Antonio M. García-García,* Hyejin Ryu, Deung-Jang Choi, Javier Zaldívar, Shujie Tang, Bo Fan, Zhi-Xun Shen, Sung-Kwan Mo, José Ignacio Pascual, and Miguel M. Ugeda*

ABSTRACT: Eigenstate multifractality is a distinctive feature of noninteracting disordered metals close to a metal–insulator transition, whose properties are expected to extend to superconductivity. While multifractality in three dimensions (3D) only develops near the critical point for specific strong-disorder strengths, multifractality in 2D systems is expected to be observable even for weak disorder. Here we provide evidence for multifractal features in the superconducting state of an intrinsic, weakly disordered single-layer NbSe₂, by means of low-temperature scanning tunneling microscopy/spectroscopy. The superconducting gap, characterized by its width, depth, and coherence peaks' amplitude, shows a characteristic spatial modulation coincident with the periodicity of the quasiparticle interference pattern. The strong spatial inhomogeneity of the superconducting gap width, proportional to the local order parameter in the weak-disorder regime, follows a log-normal statistical distribution as well as a power-law decay of the two-point correlation function, in agreement with our theoretical model. Furthermore, the experimental singularity spectrum $f(\alpha)$ shows anomalous scaling behavior typical from 2D weakly disordered systems.

KEYWORDS: STM/STS, 2D transition metal dichalcogenides, superconductivity, disorder, multifractality, quasiparticle interference.

Quantum coherence phenomena have a profound impact in the dynamics of disordered media. A paradigmatic example is the Anderson transition in disordered metals where quantum interference of noninteracting electrons induces spatial localization, leading to insulating states beyond a critical disorder strength.¹ In the vicinity of the transition preceding localization, these systems display eigenstates being neither extended nor localized that strongly fluctuate at all length scales. Such near-critical eigenstates exhibit multifractal character; i.e., they are formed by interwoven sets of different fractals, each characterized by a noninteger dimension.^{2–4} These critical eigenstates' correlations are of fundamental relevance in the presence of disorder, since the multifractal regime dominates their electronic and magnetic properties.^{5–8}

When attractive interactions between electrons are present in metals, coherent electronic states such as superconductivity (SC) can emerge in the presence of disorder. In the strong-disorder regime beyond the critical value, Anderson localization disables long-range quantum coherence, thus quenching superconductivity. For weak disorder, superconductivity persists^{9,10} even in polycrystalline or amorphous materials near the Anderson localization transition.¹¹ Nonetheless, even weak disorder strongly affects superconductivity. Recent experimental studies showed that disorder leads to spatial inhomogeneity^{10,12–14} and granularity¹⁵ in the superconducting order



parameter, in agreement with previous theoretical results.¹⁶ Despite these findings demonstrating the intricate interplay between disorder and superconductivity, the existence of the superconducting state in the multifractal regime remains unexplored, and the signatures of multifractality have been mostly theoretically addressed so far.^{17–20} Such an investigation seems particularly suitable in 2D materials since, unlike in 3D where multifractality only arises in a narrow range of disorder around criticality, multifractality is expected to emerge in 2D for a broad range of disorder strengths.^{20,21} The existence of multifractality in 2D superconductors is expected to shed light on long-standing problems such as the observed intermediate metallic state²² and variations of the superconductivity strength near the 2D limit.²³

2D is the marginal dimension for both localization and superconductivity. Scaling theory predicts that electronic eigenstates in infinite 2D systems are localized regardless of

the disorder strength²⁴ precluding the development of multifractality and superconductivity. However, this is only valid for infinite 2D systems with time reversal symmetry, and therefore, 2D systems with spin-dependent hopping exhibit a metallic ground state for sufficiently weak disorder and, thus a broad region where both multifractality and superconductivity can coexist.²⁵ 2D materials develop multifractality provided the size of the material is smaller than the localization length η , which can be extremely large in the weak-disorder regime (it scales inversely with the disorder strength, $\eta \propto l \exp(\pi k l / 2)$, where k is the wavevector and l is the mean-free path). In this arena, single-layer transition metal dichalcogenide superconductors are envisaged as ideal systems to investigate this elusive regime.

Here we provide evidence for the multifractal character of the superconducting state in single-layer NbSe₂, a 2D superconductor.²³ Intrinsic weak disorder in NbSe₂ monolayers triggers multifractality of the single-particle eigenstates, which dramatically impacts its superconducting state. By means of spatially resolved scanning tunneling spectroscopy at $T = 1.1$ K, well below T_C , we observe strong sub-nanometer-sized fluctuations in the superconducting order parameter (proportional to the SC width for weak disorder¹⁶) as well as in the coherence peak amplitude. We find that the spatial distribution of the SC order parameter amplitude corresponds to a log-normal type and, simultaneously, its spatial correlations show power-law decay for intermediate distances. Furthermore, the associated experimental singularity spectrum $f(\alpha)$ shows anomalous scaling behavior typical from 2D weakly disordered systems. These features demonstrate that superconductivity in single-layer NbSe₂ is governed by multifractal electronic states even for weak disorder.

Our experiments were performed on single-layer NbSe₂ grown on bilayer graphene (BLG)/6H-SiC(0001) as shown in Figure 1a. Atomically resolved scanning tunneling microscopy (STM) images of the hexagonal NbSe₂ films (Figure 1b) reveal high crystallinity ($< 1 \times 10^{12}$ defects/cm²), where the main source of defects are island edges and 1D grain boundaries (Figure 3b). Superconductivity in NbSe₂ is depressed in the single-layer limit ($T_C = 1.9$ K)²³ as compared to the bulk ($T_C = 7.2$ K). At $T = 1$ K, charge density wave (CDW) order is fully developed as seen in Figure 1b. STM dI/dV spectra (Figure 1c) taken at different locations of the same region exhibit a dip in the density of states (DOS) at the Fermi level (E_F) that corresponds to the superconducting gap. The features that define the SC gap, i.e. depth, width, and coherence peak amplitude, are seen to locally vary at the nanometer scale. These fluctuations were consistently observed in all the NbSe₂ regions studied regardless of shape, size and crystallinity.

To better understand the nature of the SC fluctuations in single-layer NbSe₂, we spatially mapped the width and depth of the SC gap in multiple regions with high-spatial resolution of ~ 1 Å (see the Supporting Information (SI) for the extraction procedure of the SC gap). All the regions studied here were routinely imaged with atomic resolution prior to the STS acquisition to ensure that they corresponded to monolayer regions (see Methods for a description of the procedure). The width and depth of the SC gap are a measure of the local SC order parameter amplitude for weak disorder¹⁶ and the degree of development of SC, respectively. Figure 2a shows a representative map of the spatial distribution of the width of the SC gap in a 12.4 nm \times 12.4 nm region (90 \times 90 mesh that

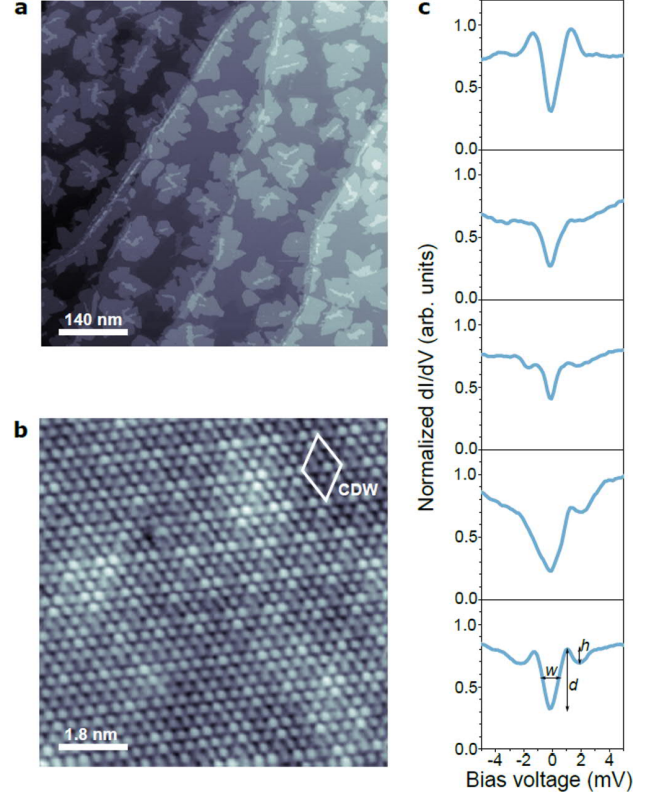


Figure 1. (a) Large-scale STM topograph of single-layer NbSe₂/BLG ($V_s = 1$ V, $I_t = 10$ pA). (b) Atomically resolved STM image of single-layer NbSe₂. The 3×3 CDW superlattice is indicated ($V_s = 14$ mV, $I_t = 1$ nA). (c) Normalized dI/dV spectra acquired at several nearby locations on NbSe₂ ($f = 938$ Hz, $I_t = 0.8$ nA, $V_{rms} = 20$ μ V). The definition of superconducting gap width, depth, and coherence peak amplitude is indicated with arrows.

yields 8100 values). The width map unveils clear spatial fluctuations of the SC order parameter in single-layer NbSe₂ within the nm-scale. Fourier transform (FFT) analysis of this width map (Figure 2b) yields a reciprocal-space ring of radius $q = 0.88 \pm 0.08$ Å⁻¹, which reveals a single wavelength of $\lambda = 7 \pm 1$ Å involved in the complex pattern of the SC fluctuations in real space. The depth of the SC gap exhibits similar spatial fluctuations with the same wavelength (Figure 2c). These nanoscale spatial variations λ are smaller than the SC coherence length for single-layer NbSe₂ ($\xi(0) \sim 10$ nm),^{26,27} which we emphasize is theoretically plausible (see the SI for an extended discussion) and was also observed in several superconductors with different dimensionalities.^{10,28–30}

To confirm the superconducting inhomogeneity in single-layer NbSe₂, we compare the spatial fluctuations of the order parameter (Figure 2a) with the spatial distribution of the amplitude of the coherence peaks (Figure 2d) acquired over the same region. The peaks' amplitude is intimately related to long-range superconducting phase coherence and directly proportional to the quasiparticles' lifetime, which can be reduced by multiple mechanisms present in reduced dimensions and by the presence of disorder.^{10,11,13,31} The maps show strong peak's amplitude fluctuations over the same length scale as that seen for the SC width and depth (7 Å), although surrounded by regions where the coherence peaks are depleted due to intrinsic disorder in the 2D superconductor. Despite these fluctuations in the phase-coherence at the

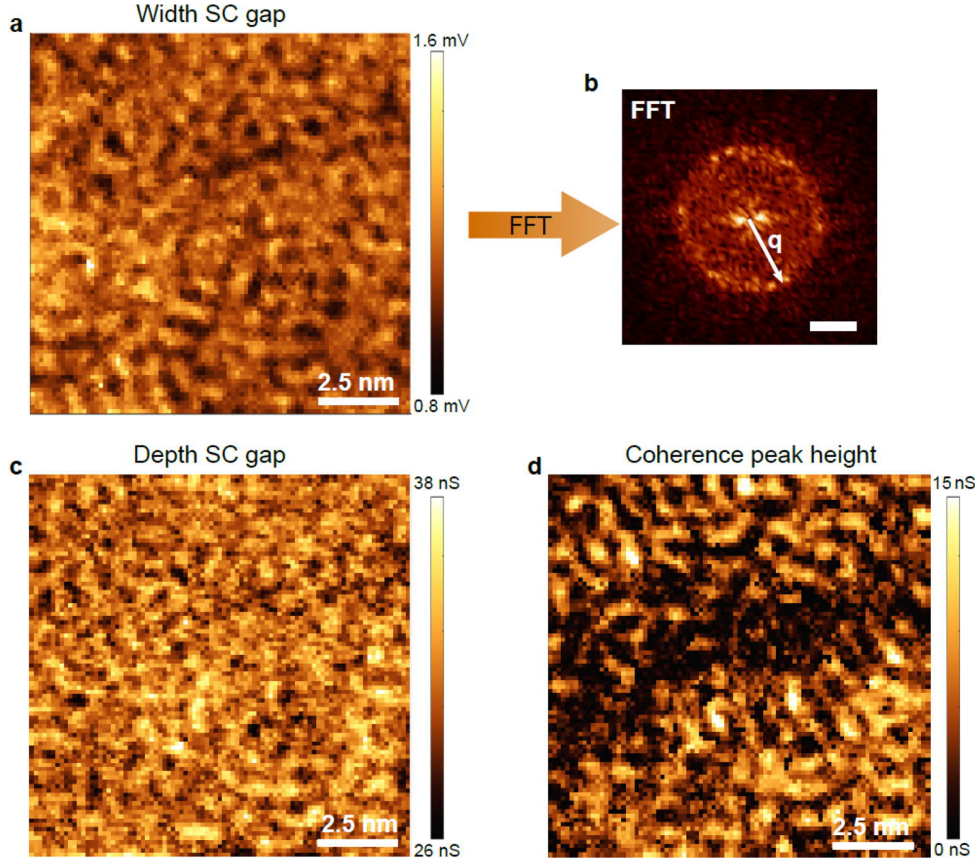


Figure 2. Spatial distribution of the superconducting gap width (a), depth (c), and coherence hole-peak amplitude (d) acquired on the same region. (b) FFT of the gap size distribution in (a). The observed q vector corresponds to a wavelength of 7 \AA . Scale bar is 0.5 \AA^{-1} .

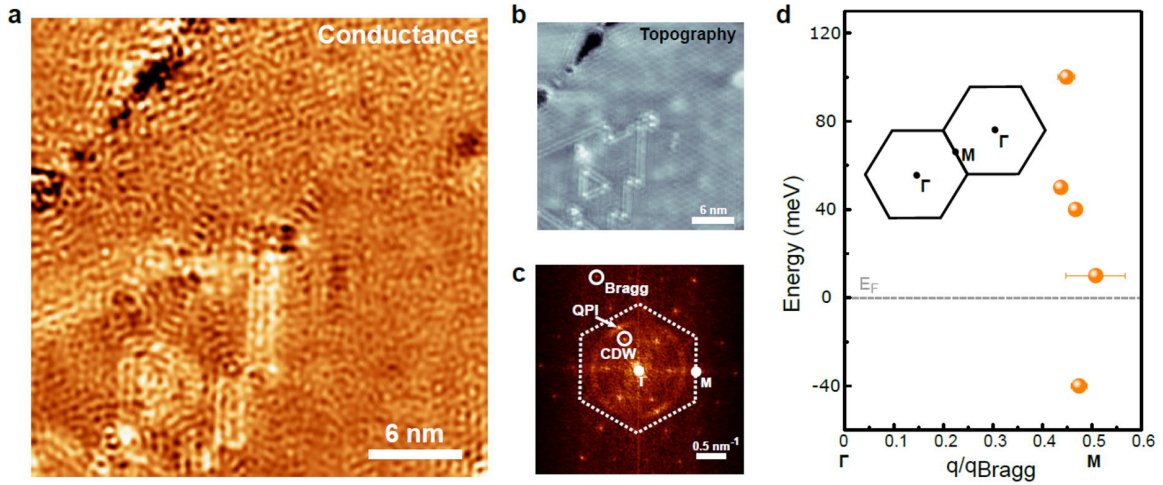


Figure 3. (a) dI/dV conductance map taken at $V_s = 40 \text{ mV}$. (b) Corresponding STM topography ($V_s = 40 \text{ mV}$, $I_t = 1 \text{ nA}$), showing the main source of intrinsic defects, i.e., 1D grain boundaries and edges. (c) FFT of the conductance map in (a). (d) Energy dependence of the QPI wavevector along the Γ -M direction extracted from the FFT of the dI/dV maps. Inset: First/second Brillouin zones.

submicron-scale, mesoscopic transport measurements in this kind of samples revealed that phase coherence holds.²³

Herein we focus on the origin of the characteristic wavelength of the SC fluctuations of $\sim 7 \text{ \AA}$. Such a wavelength does not match either the atomic lattice (3.44 \AA), the SiC reconstruction (32 \AA), or the CDW superlattice (10.3 \AA). The latter is expected since the CDW opens only on specific spots on the Nb K-H sheets, leaving most of the Fermi surface to

superconductivity.³² In order to reveal its origin, we performed spatially resolved dI/dV mapping of the electronic structure of single-layer NbSe_2 near E_F . Figure 3a shows a typical conductance map ($dI/dV(\mathbf{r}, E)$) at $V_b = +40 \text{ mV}$ in a defective region (corresponding topography in Figure 3b). Defects act as scatterers giving rise to quasiparticle interference (QPI) patterns, DOS modulations, extending tens of nanometers away from them. Figure 3c shows the Fourier analysis

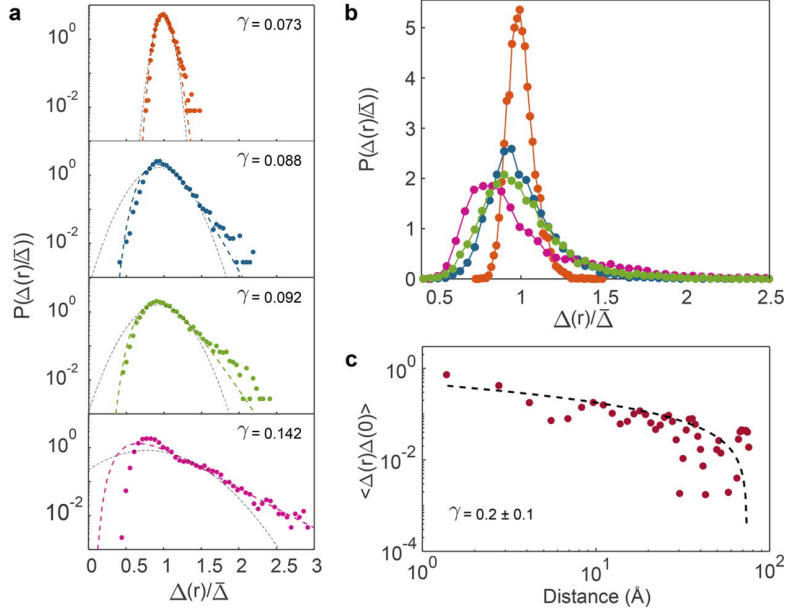


Figure 4. (a) Log-scale SC gap width probability distributions for four different studied regions of single-layer NbSe₂ with different disorder strengths ($\gamma = 1/g$, with g being the Thouless conductance), normalized to the mean value of the gap. The deviation from a Gaussian distribution (gray dashed curve) and fit to a log-normal distribution from our theoretical model (colored dashed line) indicates the multifractal character. The fitted γ value of each distribution is shown in the corresponding upper right panel. (b) Same distributions merged and shown in linear scale. (c) Two-point correlation function of the spatial SC gap width map (Figure 2a) fitted to power-law decay.

of the QPI map of Figure 3a, where an anisotropic ring with intensity maxima (\mathbf{q}_{qpi}) is present along the same ΓM direction as the dispersionless CDW signal ($\mathbf{q}_{\text{cdw}} \cong \Gamma\text{M}/3$). This feature is observable within ± 100 meV and shows a slight dispersion in k along $\Gamma\text{--M}$ (Figure 3d). The wavelength of the QPI patterns is $\lambda_{\text{QPI}} = 6.4 \pm 0.2$ Å, which nearly matches the periodicity of the SC fluctuations. This suggests that the SC fluctuations and the QPI-induced DOS modulations likely share a common origin. These QPI patterns, previously observed in bulk 2H-NbSe₂, are attributed to enhanced backscattering due to strong direction-dependent electron-phonon interactions.³³ Ab initio calculations indicate that soft acoustic phonons along the ΓM direction are strongly coupled to electrons.³⁴ This is a plausible origin of the spatial SC modulations given the significant role of acoustic phonons in the Cooper pair formation. A direct correlation between the SC modulations and DOS fluctuations, i.e., $\Delta(r) \propto \text{LDOS}$, can be ruled out due the highly dynamic conductance within the SC gap (see the SI).

Statistical analysis of the SC width values from the spatially resolved maps reveals relevant features of the SC fluctuations related to multifractality. Figure 4a (upper plot, in orange) shows the probability distribution of the SC gap width for the map shown in Figure 2a. The values fluctuate over a wide energy range of 0.8 meV around a mean value of 1.1 meV. Such a broad distribution reflects the large amplitude of the fluctuations of the SC order parameter induced in the (intrinsic) weak-disorder regime.¹⁶ Three additional experimental distributions of the SC width from regions with different degrees of intrinsic disorder are shown in Figure 4a (log scale) and b (linear scale). All of them exhibit a marked right-skewed behavior with different degrees of asymmetry. The larger the width of the distributions, the larger their asymmetry, presumably due to stronger local disorder. This marked skewness is only observed in the statistics of the SC

order parameter (SC width), with the distributions of the SC gap depth and coherence peaks being nearly symmetric and Poisson-type, respectively (see the SI).

In order to understand the characteristic properties of the SC gap distributions, we modeled single-layer NbSe₂ as a system close to the Anderson metal-insulator transition, where electronic states exhibit a multifractal character, i.e., anomalous scaling of the inverse participation ratio and a power-law decay of eigenstate correlation functions^{2,3,35} (see the SI). In 3D, where multifractality only emerges in the strong disordered limit ($\gamma = g^{-1} \sim 1$, with g being the Thouless conductance), mean field theory found that multifractality enhances the superconducting T_C .^{17,18} In 2D, where multifractality occurs in the weak-disordered regime ($\gamma \ll 1$), similar results were obtained.¹⁹ A more realistic theoretical analysis²⁰ of the spatial structure of the SC gap in 2D for $\gamma \ll 1$ found that, in agreement with previous experimental results,^{25,36} T_C was enhanced for sufficiently weak coupling, though more modestly than in earlier predictions.^{16,17} The SC gap spatial distribution is modeled by a log-normal distribution:¹⁸

$$P\left(\frac{\Delta(r)}{\bar{\Delta}}\right) = \frac{\bar{\Delta}}{\Delta(r) \sqrt{2\pi\gamma \ln(E_0/\epsilon_D)}} \times \exp\left[-\frac{\left(\ln\left(\frac{\Delta(r)}{\bar{\Delta}}\right) - \frac{3}{2}\gamma \ln(\epsilon_D/E_0)\right)^2}{2\gamma \ln(E_0/\epsilon_D)}\right] \quad (1)$$

with ϵ_D being the Debye energy, E_0 the minimum energy scale to observe multifractal eigenvector correlations, and $\bar{\Delta}$ is the average gap (see SI). Here γ is proportional to the disorder strength and eq 1 is valid for $\gamma = 4/k_F l \ll 1$ (see Methods). We use this expression to fit the statistical distributions of the SC

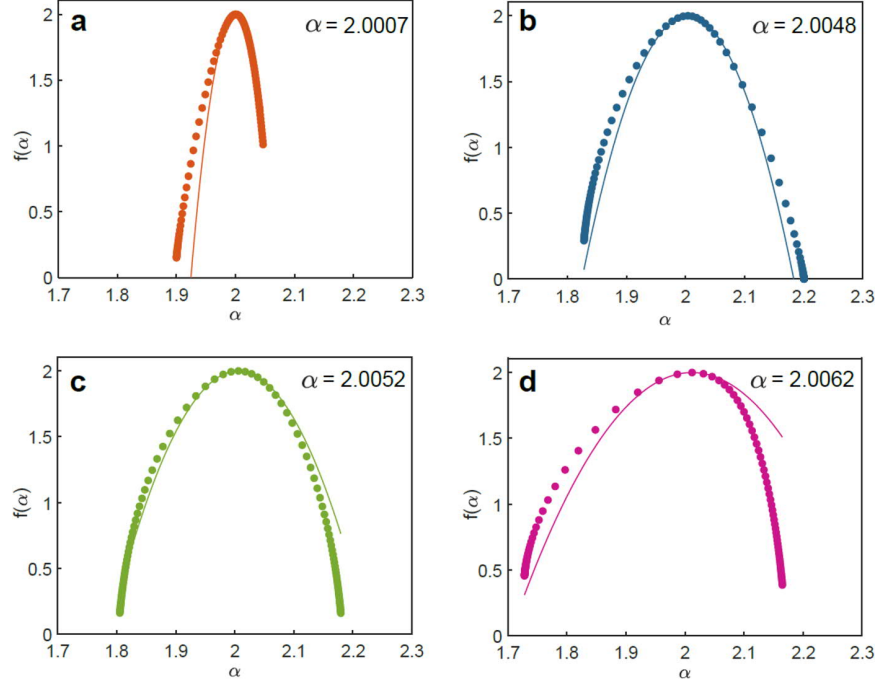


Figure 5. (a–d) Singularity spectra $f(\alpha)$ computed from the same experimental spatial distributions $\Delta(r)$ studied in Figure 4 (dots). Solid lines are the corresponding fits using the analytical prediction for a weakly disordered quasi-2D disordered system.

width maps measured in different sample regions. The theoretical SC gap $\Delta(r)$ corresponds¹⁶ to the experimental SC width in the weak disorder limit ($\gamma \ll 1$) of interest for this work. As shown in Figure 4a, the experimental right-skewed distributions of the SC width are in all cases better described by a log-normal distribution in the multifractal regime (colored dashed lines) than by a Gaussian distribution (gray dashed lines). These fits yield in all cases small γ values of ≈ 0.1 (see values in Figure 4a), which indicates that the explored NbSe₂ regions are barely defective.

A natural question that arises is whether other mechanisms could lead to log-normal distributions and whether this feature obtained from a BCS approach occurs in more realistic theoretical frameworks. First, we can rule out thermal effects since the temperature dependence of the SC gap is rather weak even beyond $T_C/2 = 1$ K. Furthermore, an indication of thermal effects would be the development of a peak in the distribution at $\Delta = 0$ corresponding to locations where the SC vanishes, which we do not observe. Thermal fluctuations beyond the employed mean field formalism are also relevant only close to T_C . We can also rule out quantum fluctuations since they are suppressed in the weak-disordered limit ($\gamma \ll 1$). Furthermore, recent calculations using the Bogoliubov de Gennes (BdG) formalism reproduce the SC gap log-normal distribution (not shown here).

To corroborate the multifractal character of the superconducting state in single-layer NbSe₂, we investigate the spatial correlations of the SC gap $\Delta(r)$, a fundamental property of the multifractal state. In addition to the log-normal distribution, another signature of multifractality is the power-law decay of eigenstate correlations for length scales larger than the mean-free path (l),³⁷ which we estimate here to be of ~ 2 nm (see Methods). Figure 4c shows the two-point spatial correlation function of the SC order parameter from the SC gap width map of Figure 2a, which is directly related to the

two-point correlation of multifractal eigenstates. The observed decay of the correlations can be fitted to a power-law function restricted to intermediate distances as (see the SI):

$$\langle \Delta(r) \Delta(r') \rangle \propto 1/|r - r'|^\gamma \quad (2)$$

with the same exponent γ that governs the decay of the multifractal eigenstates ($\gamma = 0.2 \pm 0.1$ in Figure 4c). The power-law decay is a feature present in all the studied regions for relatively long scales ($0.7 \text{ nm} < |r - r'| < 7 \text{ nm}$). The fits to power-law functions in the studied regions yield γ values that are in qualitative agreement with those independently obtained from the log-normal distributions. In agreement with our predictions,²⁰ islands with smaller γ values present a power-law decay followed by faster decay (likely exponential) for longer distances.

Lastly, the SC order parameter is expected to show multifractal features as is built up from multifractal eigenstates of the one-body problem. The singularity spectrum $f(\alpha)$ is an observable of a multifractal measure that can be computed (see the SI), and it represents the ensemble of scaling dimensions that characterize the multifractal entity. In Figure 5, we plot $f(\alpha)$ for the previously shown experimental $\Delta(r)$ distributions. In all the cases, the shape of $f(\alpha)$ is well described by a parabola, typical of multifractal eigenstates in weakly disordered 2D systems,^{35,38} which becomes broader as disorder (represented by γ) increases, suggesting an anomalous scaling in the spatial distribution of $\Delta(r)$. In the weak disorder limit at criticality, $f(\alpha)$ is exactly parabolic in the non-interacting limit and can be fitted (solid lines in Figure 5) as in refs 35 and 38. This experimental behavior, which confirms the SC order parameter as multifractal, is qualitatively reproduced by numerically computing $f(\alpha)$ for a 2D system in a random potential using the BdG equations (see the SI).

These unique features observed in the SC state of single-layer NbSe₂ must be originally triggered by the multifractal

structure of the electronic states (strictly the only fractal entity in the system).^{17–20} We have explored their nature by simultaneously mapping the conductance (LDOS) in the same regions where the SC gap was characterized. Interestingly, multifractal effects on the electronic conductance are only observable in the most disordered regions (SI, Figure S2m–p). The conductance distributions corresponding to the four regions studied in Figure 4 show Gaussian distributions for $\gamma \leq 0.16$ that evolve toward a right-skewed log-normal distribution for larger disorder ($\gamma = 0.142$). The larger sensitivity of the SC to multifractality than that of the LDOS is due to the SC gap exponential dependence on the electron–phonon coupling (V), i.e., $\Delta \propto e^{-1/2N(0)V}$, with $N(0)$ being the LDOS at E_F . Small changes in the coupling and DOS induce comparatively large changes in the SC gap for disorder regimes where the electronic states are barely multifractal and the effects in the conductance nearly imperceptible. Therefore, superconductivity amplifies the effect of multifractality and enables its observation in nearly pristine 2D superconductors.

In summary, we provide experimental evidence of the elusive multifractal superconducting state in a prototypical 2D superconductor in the low-disorder (intrinsic) regime. We demonstrate that multifractal characteristics fully manifest in the superconducting state even in the weak disorder regime. Multifractality is therefore expected to dominate the superconducting properties of the recently discovered family of highly crystalline 2D superconductors with spin–orbit coupling such as single layers of transition metal dichalcogenides. These 2D materials open the door for further investigation and eventual control of the intriguing multifractal regime.

■ METHODS

Sample Preparation and STM/STS Characterization.

Single-layer NbSe₂ was grown by molecular beam epitaxy (MBE) on epitaxial BLG on 6H-SiC(0001) at the HERS endstation of Beamline 10.0.1, Advanced Light Source, Lawrence Berkeley National Laboratory (the MBE chamber had a base pressure of $\sim 1 \times 10^{-10}$ Torr). We used SiC wafers with a resistivity of $\rho \sim 300 \text{ } \Omega\text{-cm}$. BLG substrates were obtained by flash annealing SiC(0001) substrates to $\sim 1600 \text{ K}$. High purity Nb and Se were evaporated from an electron-beam evaporator and a standard Knudsen cell, respectively. The flux ratio of Nb to Se was controlled to be $\sim 1:30$. The growth process was monitored by in situ RHEED, and the growth rate was $\sim 17 \text{ min per layer}$. During the growth, the substrate temperature was kept at 600 K , and after growth the sample was annealed to 670 K . To protect the film from contamination and oxidation during transport through air to the UHV-STM chamber, a Se capping layer with a thickness of $\sim 10 \text{ nm}$ was deposited on the sample surface after growth. For subsequent STM experiments, the Se capping layer was removed by annealing the sample to $\sim 530 \text{ K}$ in the UHV STM system for 30 min. STM imaging and STS experiments were performed in a commercial SPECS GmbH low-temperature (1.1 K) STM apparatus, under UHV conditions. STM differential conductance (dI/dV) spectra were measured at 1.1 K using standard lock-in techniques. To ensure that all the STS data were taken in monolayer regions, we routinely carried out a two-step procedure before the STS experiments consisting of the measurement of the apparent height of the chosen NbSe₂ island, which had to be $\approx 7 \text{ } \text{Å}$, which corresponds to the monolayer. Subsequent STM imaging of

the selected regions was carried out with atomic resolution to visualize the 3×3 CDW order. STM/STS data were analyzed and rendered using WSxM software.³⁹

All our STS maps were purposely carried out in regions without large defects (grain boundaries, edges, adsorbates, etc.) in the field of view (FOV) to avoid spurious electronic effects in the SC gap maps. This is typically $16 \text{ nm} \times 16 \text{ nm}$ in our samples. Since the FOV is the upper bound for the longest wavelength (λ) of the detectable SC fluctuations and the lower bound is the pixel-to-pixel distance ($\sim 1 \text{ } \text{Å}$ in the STS maps), our experimental spatial range of detection of SC fluctuations is $0.1 \text{ nm} < \lambda < 16 \text{ nm}$. As we describe in the SI, this range of detection likely comprises the relevant spatial length scales of this system and, therefore, we believe that our measurements and further statistical analysis are reliable and would not change for larger FOVs.

Mean Free Path Estimation (l). The mean free path, l , in 2D is $l = h\sigma/(e^2\sqrt{2\pi n})$, with σ and n being the conductivity and electronic density of single-layer NbSe₂, respectively. Our previous transport experiments in this type of samples showed $\sigma \approx 1/300 \text{ } \Omega$ in the normal state; therefore, $l = 24.4/\sqrt{n}$. Taking $n = 1.25 \times 10^{16} \text{ cm}^{-2}$ as in ref 27, then $l \approx 2 \text{ nm}$. This estimation may vary due to other factors such as the presence of graphene, the exact geometry of the transport devices, and the exact value of n . In ref 27, a smaller value of $l = 1.3 \text{ nm}$ is reported.

A value of $l \sim 2 \text{ nm}$ yields $\gamma = 4/k_F l = 4/(\sqrt{2\pi n})l \sim 0.07 \ll 1$, which is in good agreement with the experimental γ values extracted from our measurements. Furthermore, the condition $\gamma \sim 0.07 \ll 1$ is fulfilled, which validates the applicability of eq 1 used in the theoretical fit of the statistical distributions of the SC width maps.

■ AUTHOR INFORMATION

Corresponding Authors

Antonio M. García-García — Shanghai Center for Complex Physics, Department of Physics and Astronomy, Shanghai Jiao Tong University, Shanghai 200240, China; Email: amgg@sjtu.edu.cn

Miguel M. Ugeda — CIC nanoGUNE, 20018 Donostia-San Sebastián, Spain; Centro de Física de Materiales CFM/MPC (CSIC-UPV/EHU), 20018 San Sebastián, Spain; Donostia International Physics Center (DIPC), 20018 San Sebastián, Spain; Ikerbasque, Basque Foundation for Science, 48013 Bilbao, Spain; orcid.org/0000-0001-7913-1617; Email: mmugeda@dipc.org

Authors

Carmen Rubio-Verdú — CIC nanoGUNE, 20018 Donostia-San Sebastián, Spain; orcid.org/0000-0002-6103-7734

Hyejin Ryu — Advanced Light Source, Lawrence Berkeley National Laboratory, Berkeley, California 94720, United

States; Center for Spintronics, Korean Institute of Science and Technology, Seoul 02792, Korea; orcid.org/0000-0003-3600-9755

Deung-Jang Choi – CIC nanoGUNE, 20018 Donostia-San Sebastián, Spain; Centro de Física de Materiales CFM/MPC (CSIC-UPV/EHU), 20018 San Sebastián, Spain; Donostia International Physics Center (DIPC), 20018 San Sebastián, Spain; Ikerbasque, Basque Foundation for Science, 48013 Bilbao, Spain

Javier Zaldívar – CIC nanoGUNE, 20018 Donostia-San Sebastián, Spain

Shujie Tang – Advanced Light Source, Lawrence Berkeley National Laboratory, Berkeley, California 94720, United States; Stanford Institute for Materials and Energy Sciences, SLAC National Accelerator Laboratory, Menlo Park, California 94025, United States

Bo Fan – Shanghai Center for Complex Physics, Department of Physics and Astronomy, Shanghai Jiao Tong University, Shanghai 200240, China

Zhi-Xun Shen – Stanford Institute for Materials and Energy Sciences, SLAC National Accelerator Laboratory, Menlo Park, California 94025, United States; Geballe Laboratory for Advanced Materials, Departments of Physics and Applied Physics, Stanford University, Stanford, California 94305, United States

Sung-Kwan Mo – Advanced Light Source, Lawrence Berkeley National Laboratory, Berkeley, California 94720, United States; orcid.org/0000-0003-0711-8514

José Ignacio Pascual – CIC nanoGUNE, 20018 Donostia-San Sebastián, Spain; Ikerbasque, Basque Foundation for Science, 48013 Bilbao, Spain; orcid.org/0000-0002-7152-4747

Author Contributions

J.I.P. and M.M.U. conceived the work and designed the research strategy. C.R.-V., D.-J.C., J.Z., and M.M.U. measured the STM/STS data. C.R.-V. analyzed the STM/STS data. J.I.P. and M.M.U. supervised the STM/STS experiments and analysis. H.R. and S.T. performed the MBE growth, which was supervised by Z.-X.S. and S.-K.M. B.F. and A.M.G.-G. performed the theoretical models under the latter supervision. M.M.U. wrote the paper with help from C.R.-V. and A.M.G.-G. M.M.U. coordinated the collaboration. All authors contributed to the scientific discussion and manuscript revisions.

Notes

The authors declare no competing financial interest.

ACKNOWLEDGMENTS

We thank Claudia Ojeda-Aristizábal and Reyes Calvo for fruitful discussions. A.M.G.-G. thanks Prof. Xi Chen for illuminating discussion and for sharing unpublished work before publication. M.M.U. acknowledges support by the Spanish MINECO under Grant No. MAT2017-88377-C2-1-R and by the ERC Starting grant “LINKSPM” (Grant No. 758558). We acknowledge financial support from AEI/FEDER-EU through the Maria de Maeztu unit of excellence MDM-2016-0618. This research used resources of the Advanced Light Source, which is a DOE Office of Science User Facility under Contract No. DE-AC02-05CH11231. A.M.G.-G. acknowledges additional support from a Shanghai

talent program and from the National Natural Science Foundation of China (NSFC) (Grant number 11874259).

REFERENCES

- (1) Anderson, P. W. Absence of Diffusion in Certain Random Lattices. *Phys. Rev.* **1958**, *109*, 1492–1505.
- (2) Wegner, F. Inverse Participation Ratio in $2+\delta$ Dimensions. *Z. Phys. B: Condens. Matter Quanta* **1980**, *36*, 209–214.
- (3) Mirlin, A. D.; Evers, F. Multifractality and Critical Fluctuations at the Anderson Transition. *Phys. Rev. B: Condens. Matter Mater. Phys.* **2000**, *62*, 7920–7933.
- (4) Burmistrov, I. S.; Gornyi, I. V.; Mirlin, A. D. Multifractality at Anderson Transitions with Coulomb Interaction. *Phys. Rev. Lett.* **2013**, *111*, No. 066601.
- (5) Morgenstern, M.; Klijn, J.; Meyer, C.; Wiesendanger, R. Real-Space Observation of Drift States in a Two-Dimensional Electron System at High Magnetic Fields. *Phys. Rev. Lett.* **2003**, *90*, No. 056804.
- (6) Hashimoto, K.; Sohrmann, C.; Wiebe, J.; Inaoka, T.; Meier, F.; Hirayama, Y.; Römer, R. A.; Wiesendanger, R.; Morgenstern, M. Quantum Hall Transition in Real Space: From Localized to Extended States. *Phys. Rev. Lett.* **2008**, *101*, 256802.
- (7) Richardella, A.; Roushan, P.; Mack, S.; Zhou, B.; Huse, D. A.; Awschalom, D. D.; Yazdani, A. Visualizing Critical Correlations near the Metal-Insulator Transition in $\text{Ga}_{1-x}\text{Mn}_x\text{As}$. *Science* **2010**, *327*, 665–669.
- (8) Amin, K. R.; Ray, S. S.; Pal, N.; Pandit, R.; Bid, A. Exotic Multifractal Conductance Fluctuations in Graphene. *Commun. Phys.* **2018**, *1*, 1.
- (9) Mondal, M.; Kamlapure, A.; Chand, M.; Saraswat, G.; Kumar, S.; Jesudasan, J.; Benfatto, L.; Tripathi, V.; Raychaudhuri, P. Phase Fluctuations in a Strongly Disordered S-Wave NbN Superconductor Close to the Metal-Insulator Transition. *Phys. Rev. Lett.* **2011**, *106*, No. 047001.
- (10) Brun, C.; Cren, T.; Cherkez, V.; Debontridder, F.; Pons, S.; Fokin, D.; Tringides, M. C.; Bozhko, S.; Ioffe, L. B.; Altshuler, B. L.; Roditchev, D. Remarkable Effects of Disorder on Superconductivity of Single Atomic Layers of Lead on Silicon. *Nat. Phys.* **2014**, *10*, 444–450.
- (11) Sacépé, B.; Dubouchet, T.; Chapelier, C.; Sanquer, M.; Ovadia, M.; Shahar, D.; Feigel'Man, M.; Ioffe, L. Localization of Preformed Cooper Pairs in Disordered Superconductors. *Nat. Phys.* **2011**, *7*, 239.
- (12) Lemarié, G.; Kamlapure, A.; Bucheli, D.; Benfatto, L.; Lorenzana, J.; Seibold, G.; Ganguli, S. C.; Raychaudhuri, P.; Castellani, C. Universal Scaling of the Order-Parameter Distribution in Strongly Disordered Superconductors. *Phys. Rev. B: Condens. Matter Mater. Phys.* **2013**, *87*, 184509.
- (13) Noat, Y.; Cherkez, V.; Brun, C.; Cren, T.; Carbillet, C.; Debontridder, F.; Ilin, K.; Siegel, M.; Semenov, A.; Hübers, H.-W.; Roditchev, D. Unconventional Superconductivity in Ultrathin Superconducting NbN Films Studied by Scanning Tunneling Spectroscopy. *Phys. Rev. B: Condens. Matter Mater. Phys.* **2013**, *88*, No. 014503.
- (14) Sacépé, B.; Chapelier, C.; Baturina, T. I.; Vinokur, V. M.; Baklanov, M. R.; Sanquer, M. Disorder-Induced Inhomogeneities of the Superconducting State Close to the Superconductor-Insulator Transition. *Phys. Rev. Lett.* **2008**, *101*, 157006.
- (15) Trivedi, N.; Loh, Y. L.; Bouadim, K.; Randeria, M. Emergent Granularity and Pseudogap near the Superconductor-Insulator Transition. *J. Phys. Conf. Ser.* **2012**, *376*, 012001.
- (16) Ghosal, A.; Randeria, M.; Trivedi, N. Role of Spatial Amplitude Fluctuations in Highly Disordered S-Wave Superconductors. *Phys. Rev. Lett.* **1998**, *81*, 3940.
- (17) Feigel'man, M. V.; Ioffe, L. B.; Kravtsov, V. E.; Yuzbashyan, E. A. Eigenfunction Fractality and Pseudogap State near the Superconductor-Insulator Transition. *Phys. Rev. Lett.* **2007**, *98*, No. 027001.
- (18) Feigel'man, M. V.; Ioffe, L. B.; Kravtsov, V. E.; Cuevas, E. Fractal Superconductivity near Localization Threshold. *Ann. Phys.* **2010**, *325*, 1390.

- (19) Burmistrov, I. S.; Gornyi, I. V.; Mirlin, A. D. Enhancement of the Critical Temperature of Superconductors by Anderson Localization. *Phys. Rev. Lett.* **2012**, *108*, No. 017002.
- (20) Mayoh, J.; García-García, A. M. Global Critical Temperature in Disordered Superconductors with Weak Multifractality. *Phys. Rev. B: Condens. Matter Mater. Phys.* **2015**, *92*, 174526.
- (21) Cuevas, E.; Kravtsov, V. E. Two-Eigenfunction Correlation in a Multifractal Metal and Insulator. *Phys. Rev. B: Condens. Matter Mater. Phys.* **2007**, *76*, 235119.
- (22) Saito, Y.; Kasahara, Y.; Ye, J.; Iwasa, Y.; Nojima, T. Metallic Ground State in an Ion-Gated Two-Dimensional Superconductor. *Science* **2015**, *350*, 409–413.
- (23) Ugeda, M. M.; Bradley, A. J.; Zhang, Y.; Onishi, S.; Chen, Y.; Ruan, W.; Ojeda-Aristizabal, C.; Ryu, H.; Edmonds, M. T.; Tsai, H.-Z.; Riss, A.; Mo, S.-K.; Lee, D.; Zettl, A.; Hussain, Z.; Shen, Z.-X.; Crommie, M. F. Characterization of Collective Ground States in Single-Layer NbSe₂. *Nat. Phys.* **2016**, *12*, 92–97.
- (24) Abrahams, E.; Anderson, P. W.; Licciardello, D. C.; Ramakrishnan, T. V. Scaling Theory of Localization: Absence of Quantum Diffusion in Two Dimensions. *Phys. Rev. Lett.* **1979**, *42*, 673–676.
- (25) Zhao, K.; Lin, H.; Xiao, X.; Huang, W.; Yao, W.; Yan, M.; Xing, Y.; Zhang, Q.; Li, Z.-X.; Hoshino, S.; Wang, J.; Zhou, S.; Gu, L.; Bahramy, M. S.; Yao, H.; Nagaosa, N.; Xue, Q.-K.; Law, K. T.; Chen, X.; Ji, S.-H. Disorder-Induced Multifractal Superconductivity in Monolayer Niobium Dichalcogenides. *Nat. Phys.* **2019**, *15*, 904.
- (26) Xing, Y.; Zhao, K.; Shan, P.; Zheng, F.; Zhang, Y.; Fu, H.; Liu, Y.; Tian, M.; Xi, C.; Liu, H.; Feng, J.; Lin, X.; Ji, S.; Chen, X.; Xue, Q. K.; Wang, J. Ising Superconductivity and Quantum Phase Transition in Macro-Size Monolayer NbSe₂. *Nano Lett.* **2017**, *17*, 6802–6807.
- (27) Wang, H.; Huang, X.; Lin, J.; Cui, J.; Chen, Y.; Zhu, C.; Liu, F.; Zeng, Q.; Zhou, J.; Yu, P.; Wang, X.; He, H.; Tsang, S. H.; Gao, W.; Suenaga, K.; Ma, F.; Yang, C.; Lu, L.; Yu, T.; Teo, E. H. T.; Liu, G.; Liu, Z. High-Quality Monolayer Superconductor NbSe₂ Grown by Chemical Vapour Deposition. *Nat. Commun.* **2017**, *8*, 394.
- (28) Pan, S. H.; O’Neal, J. P.; Badzey, R. L.; Chamon, C.; Ding, H.; Engelbrecht, J. R.; Wang, Z.; Eisaki, H.; Uchida, S.; Gupta, A. K.; Ng, K. W.; Hudson, E. W.; Lang, K. M.; Davis, J. C. Microscopic Electronic Inhomogeneity in the High-Tc Superconductor Bi₂Sr₂CaCu₂O_{8+x}. *Nature* **2001**, *413*, 282–285.
- (29) Bose, S.; García-García, A. M.; Ugeda, M. M.; Urbina, J. D.; Michaelis, C. H.; Brihuega, I.; Kern, K. Observation of Shell Effects in Superconducting Nanoparticles of Sn. *Nat. Mater.* **2010**, *9*, 550–554.
- (30) Hamidian, M. H.; Edkins, S. D.; Joo, S. H.; Kostin, A.; Eisaki, H.; Uchida, S.; Lawler, M. J.; Kim, E. A.; Mackenzie, A. P.; Fujita, K.; Lee, J.; Davis, J. C. S. Detection of a Cooper-Pair Density Wave in Bi₂Sr₂CaCu₂O_{8+x}. *Nature* **2016**, *532*, 343–347.
- (31) Bouadim, K.; Loh, Y. L.; Randeria, M.; Trivedi, N. Single- and Two-Particle Energy Gaps across the Disorder-Driven Superconductor-Insulator Transition. *Nat. Phys.* **2011**, *7*, 884–889.
- (32) Rahn, D. J.; Hellmann, S.; Källäne, M.; Sohr, C.; Kim, T. K.; Kipp, L.; Rossnagel, K. Gaps and Kinks in the Electronic Structure of the Superconductor 2H-NbSe₂ from Angle-Resolved Photoemission at 1 K. *Phys. Rev. B: Condens. Matter Mater. Phys.* **2012**, *85*, 224532.
- (33) Arguello, C. J.; Rosenthal, E. P.; Andrade, E. F.; Jin, W.; Yeh, P. C.; Zaki, N.; Jia, S.; Cava, R. J.; Fernandes, R. M.; Millis, A. J.; Valla, T.; Osgood, R. M.; Pasupathy, A. N. Quasiparticle Interference, Quasiparticle Interactions, and the Origin of the Charge Density Wave in 2H-NbSe₂. *Phys. Rev. Lett.* **2015**, *114*, No. 037001.
- (34) Weber, F.; Rosenkranz, S.; Castellani, J. P.; Osborn, R.; Hott, R.; Heid, R.; Bohnen, K. P.; Egami, T.; Said, A. H.; Reznik, D. Extended Phonon Collapse and the Origin of the Charge-Density Wave in 2H-NbSe₂. *Phys. Rev. Lett.* **2011**, *107*, 107403.
- (35) Castellani, C.; Peliti, L.; Castro, C. Di. On the Upper Critical Dimension in Anderson Localisation. *J. Phys. A: Math. Gen.* **1986**, *19*, L1099–L1103.
- (36) Deutscher, G.; Fenichel, H.; Gershenson, M.; Grünbaum, E.; Ovadyahu, Z. Transition to Zero Dimensionality in Granular Aluminum Superconducting Films. *J. Low Temp. Phys.* **1973**, *10*, 231.
- (37) Mirlin, A. D. Statistics of Energy Levels and Eigenfunctions in Disordered Systems. *Phys. Rep.* **2000**, *326*, 259–382.
- (38) Cuevas, E. F(α) Multifractal Spectrum at Strong and Weak Disorder. *Phys. Rev. B: Condens. Matter Mater. Phys.* **2003**, *68*, No. 024206.
- (39) Horcas, I.; Fernández, R.; Gómez-Rodríguez, J. M.; Colchero, J.; Gómez-Herrero, J.; Baro, A. M. WSXM: A Software for Scanning Probe Microscopy and a Tool for Nanotechnology. *Rev. Sci. Instrum.* **2007**, *78*, No. 013705.